



# Preparation and characterization of an amine-modified graphene aerogel for enhanced carbon dioxide adsorption

Jingjie Wu<sup>1</sup>, Xianyu Qiu<sup>1</sup>, and Shuixia Chen<sup>1,2,\*</sup>

<sup>1</sup>PCFM Lab, School of Chemistry, Sun Yat-Sen University, Guangzhou 510275, People's Republic of China

<sup>2</sup>Materials Science Institute, Sun Yat-Sen University, Guangzhou 510275, People's Republic of China

Received: 20 June 2021

Accepted: 27 November 2021

Published online:

3 January 2022

© The Author(s), under exclusive licence to Springer Science+Business Media, LLC, part of Springer Nature 2021

## ABSTRACT

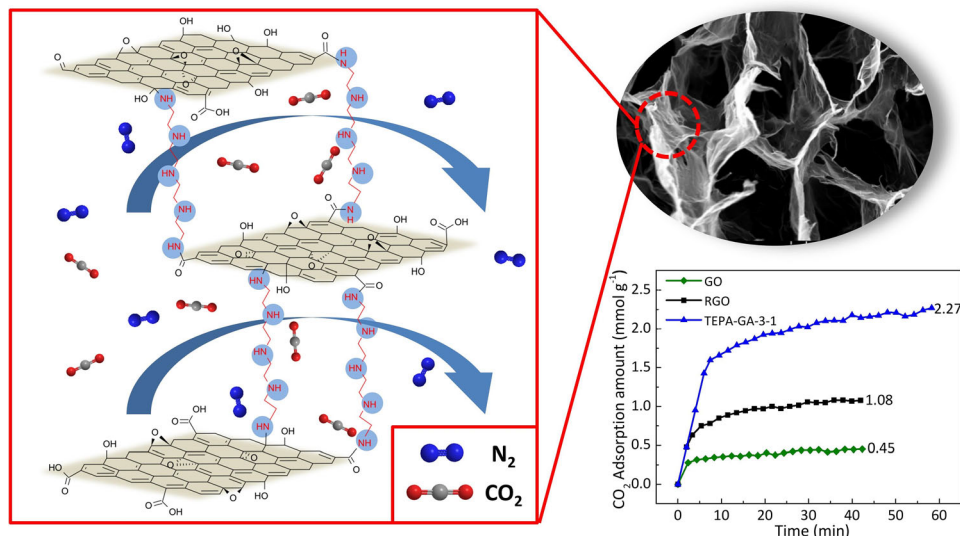
A 3D porous graphene aerogel (GA) was prepared via one-step hydrothermal method and freeze-drying technology, in which organic amine reagents were used as cross-linker to combine the graphene oxide (GO) sheets. With abundant amino groups, the organic amine reagents also acted as adsorption sites to improve CO<sub>2</sub> adsorption capacity. Morphology, pore structure and surface chemical structure of the as-prepared materials were characterized by SEM, FTIR, XRD, Raman, TG, N<sub>2</sub> adsorption–desorption. CO<sub>2</sub> adsorption performance was evaluated by dynamic adsorption experiments in a fixed-bed column. Aminated by tetraethylenepentamine (TEPA), the prepared 3D graphene aerogel (TEPA-GA-3–1) achieved a CO<sub>2</sub> adsorption capacity as high as 2.27 mmol g<sup>-1</sup> at 25 °C, 0.1 bar, which was attributed to its developed porous structure and high amino density. Further, the existence of water could improve the CO<sub>2</sub> adsorption amount because H<sub>2</sub>O directly participates the reaction of CO<sub>2</sub> with amine to form bicarbonates. The prepared GA adsorbent also exhibited good stability after six adsorption–desorption cycles. The above result suggests that amine-modified graphene aerogel has a potential application for CO<sub>2</sub> capture from flue gas.

Handling Editor: Dale Huber.

Address correspondence to E-mail: cescsx@mail.sysu.edu.cn

<https://doi.org/10.1007/s10853-021-06768-3>

## GRAPHICAL ABSTRACT



## Introduction

The global climate problem caused by the greenhouse effect has become a serious survival challenge facing mankind since the beginning of the twenty-first century [1]. At the same time, the concentration of  $\text{CO}_2$  in the atmosphere has increased rapidly since the industrial revolution, which is considered as the major reason for greenhouse effect [2]. In order to reduce the emission of carbon dioxide,  $\text{CO}_2$  capture and storage technology (CCS) [3] is developed rapidly. Nowadays, there are lots of  $\text{CO}_2$  capture methods including absorption [4], adsorption [5], membrane separation technology [6] and so forth. Among them, adsorption technology shows better economic benefit and industrial development prospects because of low cost, low regeneration energy consumption and wide temperature range for application [7].

It is critical to select the suitable adsorbent for  $\text{CO}_2$  adsorption. At present, various porous adsorbents, such as carbon materials [8], molecular sieves [9], silicon materials [10] and metal–organic skeleton materials [11], have been studied extensively. As an important member of carbon materials, graphene has attracted much attention since its discovery due to its

excellent mechanical properties, large specific surface area and unique two-dimensional planar structure [12, 13]. However, pure graphene mainly adsorbs gas through physical interaction by its porous structure, showing a relatively low adsorption capacity, which is not suitable for preparation of  $\text{CO}_2$  adsorbent. Graphene oxide (GO), an important derivative of graphene [14], possesses a large number of oxygen-containing groups on the structure, able to provide adequate reaction sites for its further functionalization. Graphene-based adsorbents with controllable morphology and excellent properties can be prepared by functionalizing GO [15, 16]. In this regard, surface modification on GO with corresponding basic compounds or compounds containing basic groups (such as amine) can effectively enhance the  $\text{CO}_2$  adsorption capacity of the modified GO. For example, Zhao et al. [17] prepared an aminated graphene oxide as  $\text{CO}_2$  adsorbents by using ethylenediamine (EDA). Its  $\text{CO}_2$  adsorption capacity was  $46.55 \text{ mg g}^{-1}$  (equally  $1.06 \text{ mmol g}^{-1}$ ) at  $30^\circ\text{C}$ , 15%  $\text{CO}_2$ . Using 3-aminopropyl-triethoxysilane (APTES) as modifier, Jeewan Pokhrel et al. [18] prepared the GO-based solid amine adsorbent; its adsorption capacity of  $\text{CO}_2$  was  $1.5 \text{ mmol g}^{-1}$  at 1 bar. However, two-dimensional graphene materials are easy to stack during modification and use, which limits the surface area and

effective amine loading, thus restricting the adsorption capacity of CO<sub>2</sub>. Therefore, establishing porous structure is an effective measure to improve the adsorption performance of graphene-based materials [19].

Recently, three-dimensional (3D) graphene-based materials trigger tremendous technological and scientific interests for its merit of low mass transfer resistance, porous structure, the large specific surface area [20]. 3D macrostructures not only can provide larger specific area for physical adsorption but also more active sites for chemical adsorption.

In this study, we reported the preparation of a 3D graphene aerogel by using different organic amine reagents as cross-linker to combine the GO sheets. Here, organic amine reagents also acted as adsorption sites for enhanced CO<sub>2</sub> capture due to containing abundant amino groups. The effects of the amount of the cross-linker, amination reagents type and humidity on the CO<sub>2</sub> adsorption capacity were explored. In addition, regeneration performance was also tested.

## Experimental

### Materials and reagents

Graphene oxide (GO) was purchased from Nanjing Xianfeng Nanomaterials technology company, China. Tetraethylenepentamine (TEPA) and triethylenetetramine (TETA) were purchased from Fuchen Reagent Company (Tianjin, China). Polyethyleneimine (PEI, Mw = 600) was bought from Aladdin Industrial Corporation (Shanghai, China). Sodium hydroxide was obtained from Guangzhou Reagent Company (Guangdong, China). All chemicals were used without further purification. Distilled water was used to prepare all solution in this study.

### Synthesis of amine-modified graphene aerogel

The preparation of the amine-modified graphene aerogel was modified according to previous literature [21]. In a typical preparation process, 0.2 g GO was ultra-sonicated in 50 mL distilled water to obtain GO aqueous dispersion. The pH of the dispersion was adjusted to 8 by adding 0.1 M sodium hydroxide solution dropwise. Different amount of amine

reagent (for example, TEPA) was added into the GO dispersion, and then, the mixture was put in a sealed Teflon-lined stainless-steel autoclave after stirring. Next, the autoclave was placed in an oven for hydrothermally reaction at 180 °C for 12 h. After cooling down to ambient temperature, the product was taken out and washed by distilled water until the pH was neutral. The prepared hydrogel was frozen by liquid nitrogen and then freeze-dried for 48 h to obtain the TEPA-GO aerogels (TEPA-GO). With TEPA as the cross-linker, the as-prepared aerogel was named as TEPA-GA-X-1, where X referred to the mass ratio of TEPA to GO. The preparation scheme is illustrated in Figure 1. Reduced graphene oxide (RGO) aerogel was synthesized in the same experimental process without adding TEPA.

### Characterization of materials

The morphology of the prepared adsorbent was observed by Scanning electron microscope (SEM, S4800, Hitachi, Japan). The Fourier transform infrared spectra (FTIR, Tensor-27, Bruker, Germany) were used to characterize the functional groups on adsorbent in the wavenumber range from 4000 to 400 cm<sup>-1</sup>. The elemental composition of aerogels was measured by using an elemental analysis analyzer (EA, Elementar Vario EL, Germany). N<sub>2</sub> adsorption–desorption isotherm and pore size distribution of the sample were measured with an automatic gas adsorption instrument (ASAP2020, Micromeritics Corp, USA) at 77 K at the range of relative pressure from 10<sup>-6</sup> to 1. Specific surface area and pore parameters were calculated by using the Brunauer–Emmett–Teller (BET) method and density functional theory (DFT) method, separately. The Raman spectra (Nicolet NXR9650, USA) were applied to characterize the chemical structure of the samples in the range of 1000–2000 cm<sup>-1</sup>. X-ray diffraction (XRD) patterns of the samples were measured from 5° to 45° by the X-ray diffraction instrument (D8 ADVANCE, Bruker, Germany).

### CO<sub>2</sub> adsorption experiment

The CO<sub>2</sub> adsorption capacity was measured in a fixed bed flow system. Before the adsorption test, the sample was dried at 70 °C for 24 h. In the adsorption process, the adsorbent was placed in a glass column ( $\phi=1.5$  cm). Then, the sample was purged with dried N<sub>2</sub> flow for 20 min to remove the ambient air. After

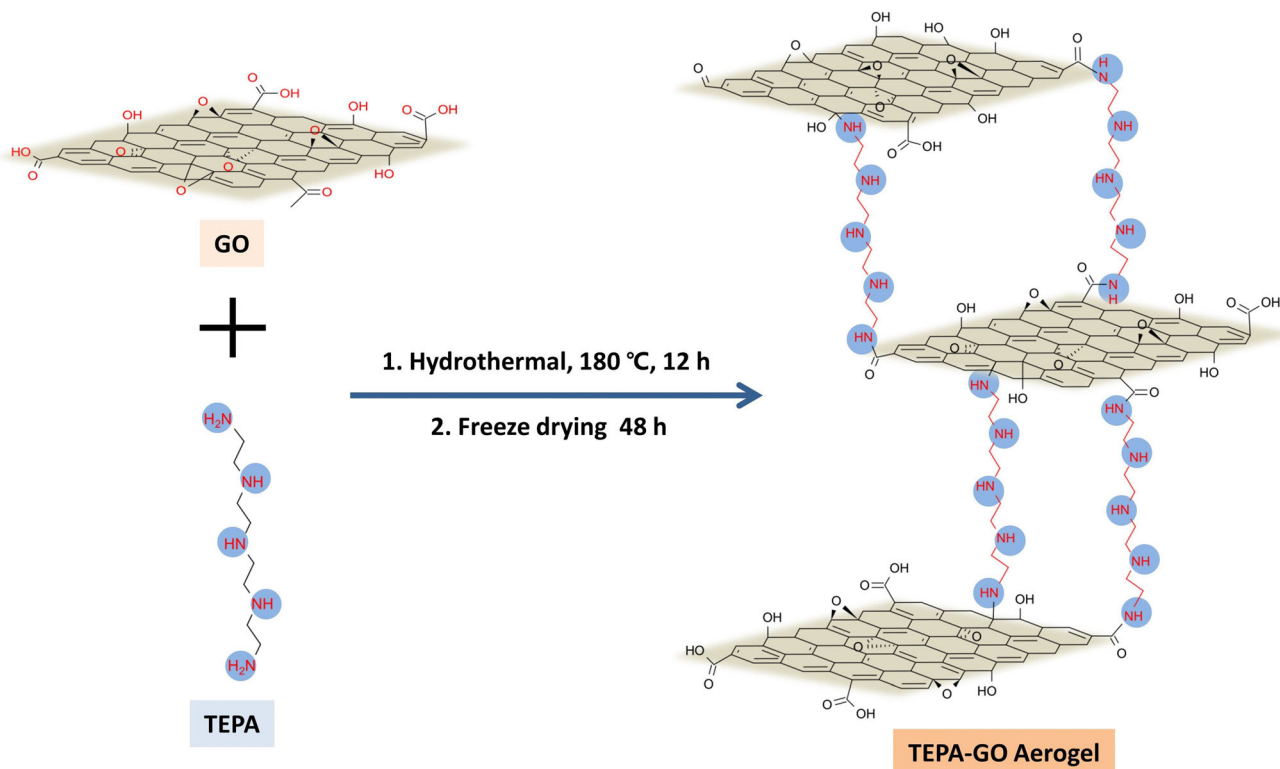


**Figure 1** Schematic diagram of preparation of amine-modified aerogels.

that a mixture gas of CO<sub>2</sub> (10 vol%) and N<sub>2</sub> (90 vol%) was introduced at a flow rate of 30 mL/min for the adsorption evaluation. The influent/effluent CO<sub>2</sub> concentration was tested every two minutes by using the gas chromatography (Techcomp 7900, China) with a thermal conductivity detector (TCD). Based on breakthrough curves, CO<sub>2</sub> adsorption amount of the sample could be calculated. After completing CO<sub>2</sub> adsorption, the adsorbent was regenerated by purged with a flow rate of 30 mL/min N<sub>2</sub> at 90 °C for 30 min.

The CO<sub>2</sub> adsorption capacity was calculated by the following equation:

$$Q = \int_0^t (C_{in} - C_{eff}) V dt / 22.4 W \quad (1)$$

where  $Q$  represents the adsorption capacity of the adsorbent (mmol CO<sub>2</sub> g<sup>-1</sup>);  $t$  is the adsorption time (min);  $C_{in}$  and  $C_{eff}$  are the influent and effluent concentrations of CO<sub>2</sub> (mL min<sup>-1</sup>), respectively;  $V$  is the total flow rate, 30 mL/min;  $W$  represents the weight of the adsorbent (g); and 22.4 is the molar volume of gas (mL mmol<sup>-1</sup>).

## Results and discussion

### Structure characterization of graphene-based aerogels

It is well known that there are various oxygenated functional groups on the GO sheets, which can react with amino groups through amidation or ring opening reaction under appropriate condition. Figure 2 depicts the functional groups of GO, RGO, TEPA-GA by means of FT-IR spectra. For the pristine GO, the prominent peaks (shown in Figure 2a) at 1720 cm<sup>-1</sup> and 1610 cm<sup>-1</sup> could be ascribed to the C=O and aromatic C=C stretching vibrations [22]. A broad absorption peak was observed at 3000–3400 cm<sup>-1</sup> due to the O-H stretching vibration [23] and the absorbed water vapor from the air. Besides, the bands appeared at 1230 cm<sup>-1</sup> and 1050 cm<sup>-1</sup> were attributed to the symmetric stretching and deformation vibrations of epoxy groups. Comparing TEPA-GA with GO and RGO, new absorption peaks were observed at 1650 and 1560 cm<sup>-1</sup>, corresponding to the stretching vibration of amide bond and the bending vibration of N-H [24], which successfully demonstrated that TEPA had reacted with carboxyl on the

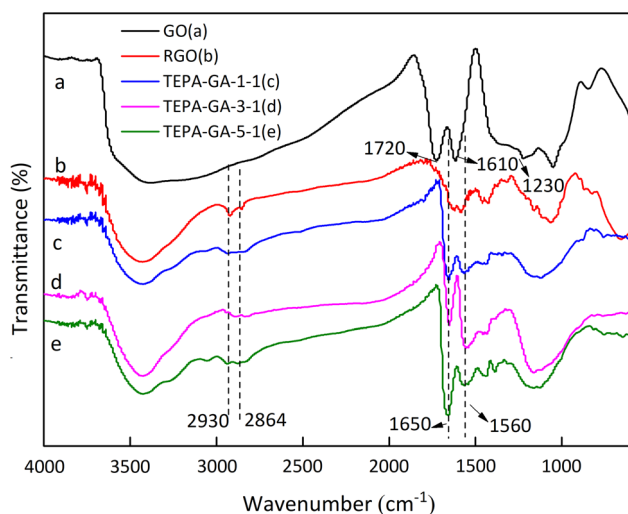


**Figure 2** FT-IR spectra of **a** GO, **b** RGO, **c** TEPA-GA-1-1, **d** TEPA-GA-3-1, **e** TEPA-GA-5-1.

GO sheets. Further, two peaks found at  $2930\text{ cm}^{-1}$  and  $2864\text{ cm}^{-1}$  were assignable to asymmetric and symmetric stretching modes of  $\text{CH}_2$  of TEPA [25].

The elemental analysis (Table 1) was carried out to characterize the elementary composition of the samples. It could be seen that the contents of nitrogen on GO and RGO were almost zero. After amination by TEPA, it increased significantly, growing in step with the ratio of TEPA to GO, which suggested a successful reaction between TEPA and GO.

XRD patterns are recorded in Figure 3. The strong and sharp diffraction peak of GO (Figure 3a) at  $2\theta = 10.14^\circ$  (002) showed that the crystal regularity is high. Calculated by Bragg equation [26], the interplanar spacing of GO is 8.7 Å, which is larger than that of natural graphite [27]. It is the intercalation of oxygen-containing group and water molecule that enlarges the interplanar spacing of GO. After hydrothermal reaction, the peak at  $10.14^\circ$  disappeared but a weak and broad one at around  $23^\circ$  appeared in the XRD curve of TEPA-GA because of

**Table 1** Summary of the elemental analysis of all the samples

Samples	C (wt%)	H (wt%)	N (wt%)
GO	45.32	0.85	0.00
RGO	75.69	1.54	0.30
TEPA-GA-1-1	71.28	3.93	9.00
TEPA-GA-3-1	71.83	4.04	11.15
TEPA-GA-5-1	62.01	5.11	15.82

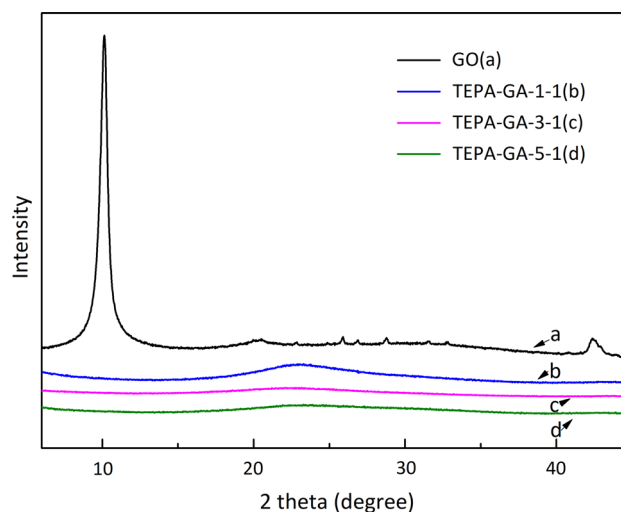


**Figure 3** XRD patterns of GO and TEPA-GO aerogels.

the amorphous structure, indicating the partial reduction of GO [28]. Furthermore, it is reported that additional defects will be produced if strong bonding between GO and attached molecules is created, thus weakening the structure of GO [29].

Additionally, the structures of GO and TEPA-GA were analyzed by Raman spectra. As shown in Figure 4, there were two characteristic peaks, located at  $1352\text{ cm}^{-1}$  and  $1592\text{ cm}^{-1}$ , both existing in GO and TEPA-GO aerogels. D band ( $1352\text{ cm}^{-1}$ ) refers to the  $\text{sp}^3$  carbon atoms of the defect structure, while G band ( $1592\text{ cm}^{-1}$ ) represents  $\text{sp}^2$  hybridized carbon atoms from the aromatic structure [30]. The D-band/G-band intensity ratios of TEPA-GO aerogels were larger than GO, indicating the increase of defects in

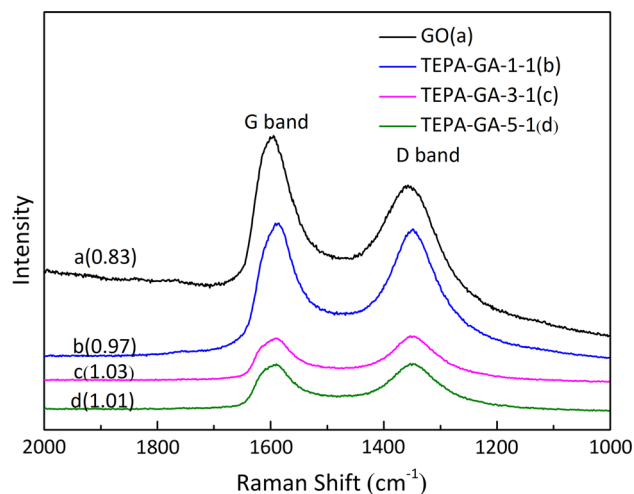


**Figure 4** Raman spectra of GO and TEPA-GO aerogels (Values in brackets are  $I_D/I_G$  ratios).



TEPA-GA, which is consistent with the analysis of XRD.

The porous properties of GO, RGO and TEPA-GO aerogels were characterized by  $N_2$  adsorption–desorption isotherms (Figure 5). It is observed that the aerogels showed a typical type-IV adsorption isotherm, indicating that the aerogels had mesoporous structure [31]. The pore size distribution shown in Figure 5b further verified the existence of mesopores. Besides, there were also lots of micropores and macropores in the prepared aerogels coming from cross-linking and freeze drying, illustrating that the aerogels were hierarchical porous structure materials. The pore parameters including BET surface area, total pore volume and average pore diameter are listed in Table 2. For the raw material GO, its BET surface area was merely  $12 \text{ m}^2 \text{ g}^{-1}$  and it had a lower pore volume of  $0.02 \text{ cm}^3 \text{ g}^{-1}$ . Compared with GO, RGO ( $168 \text{ m}^2 \text{ g}^{-1}$ ) and TEPA-GO aerogels ( $15$  to  $74 \text{ m}^2 \text{ g}^{-1}$ ), both showed a larger BET surface area. The enhancement of the BET surface area could be attributed to the cross-linking between TEPA and GO, which prevented GO sheets from stacking. It is worth noting that the BET surface area decreased as the amount of TEPA increased continuously. This phenomenon can be explained that excess TEPA may fill the micropores and mesopores of the aerogels, leading to a rapid decrease of the BET surface area [32]. These porous morphologies were clearly observed by SEM images (Figure 6). As it is shown in the micrographs, severe agglomeration appeared in GO while the aerogels showed three-dimensional porous morphology, which were in accordance with the results of pore parameters analysis.

To assess the thermal stability of the materials, thermal gravimetric analysis (TG) was carried out with heating range from 25 to  $800 \text{ }^\circ\text{C}$  under  $N_2$  flow. As it is shown in Figure 7, TG curves of all samples had a slight weight loss below  $100 \text{ }^\circ\text{C}$  as a result of physical adsorption of water and  $\text{CO}_2$  [33]. RGO exhibited excellent thermal stability with the least weight loss. After the addition of TEPA, an obvious weight loss occurred in TEPA-GA, and became more serious with the increased content of TEPA, which is due to the decrease ratio of GO to TEPA.

### Effect of organic amine type and loading amount on $\text{CO}_2$ adsorption behavior

In order to study the effect of amine type on  $\text{CO}_2$  adsorption performance of adsorbent, a number of amine-modified graphene aerogels were prepared by fixing the mass ratio of organic amine to GO at the same value of 3:1. The aerogels prepared by using TETA, TEPA, PEI ( $M_w = 600$ ) as cross-linker are labeled as TETA-GA-3-1, TEPA-GA-3-1 and PEI-GA-3-1, respectively. Figure 8 shows the  $\text{CO}_2$  adsorption breakthrough curves and adsorption amounts of different amine-modified graphene aerogels. It could be obviously seen that PEI-GA-3-1 had the shortest breakthrough time and the lowest  $\text{CO}_2$  adsorption amount ( $1.04 \text{ mmol g}^{-1}$ ). In contrast, TEPA-GA-3-1 showed the longest breakthrough time and its  $\text{CO}_2$  adsorption amount reached  $2.27 \text{ mmol g}^{-1}$ . It is because that compared with PEI, TEPA has a suitable molecular chain length and moderate viscosity [24], endowing higher reactivity for the cross-linking between GO sheets. The element analysis shown in Table 3 further proved the ideas above, where TEPA-

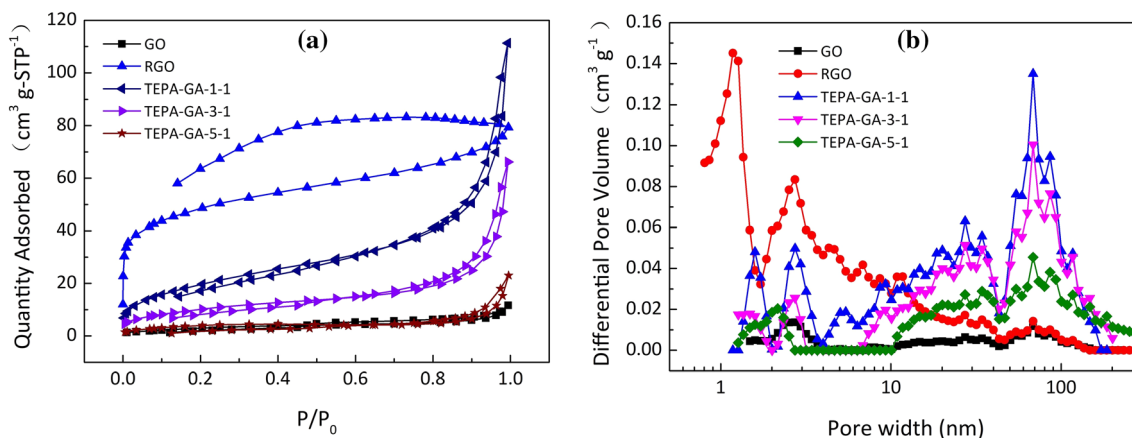


**Figure 5** The  $N_2$  adsorption–desorption isotherms **a** and BJH pore size distributions **b** of GO, RGO and TEPA-GO aerogels.

**Table 2** Summary of pore parameters of all the samples

Samples	$S_{BET}$ ( $m^2 g^{-1}$ )	$V_{Total}$ ( $cm^3 g^{-1}$ )	$D_{Pore}$ (nm)
GO	12	0.02	6.09
RGO	168	0.12	2.91
TEPA-GA-1-1	74	0.17	9.32
TEPA-GA-3-1	37	0.10	10.82
TEPA-GA-5-1	15	0.04	9.17

**Figure 6** The SEM images of GO (a), RGO (b), TEPA-GA-1-1 (c) and TEPA-GA-3-1 (d).

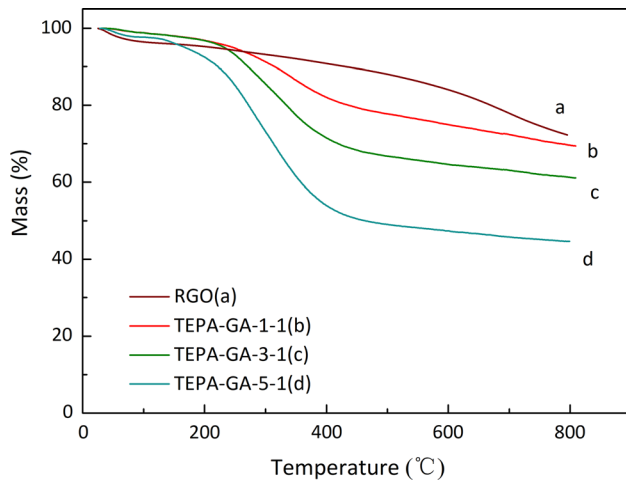
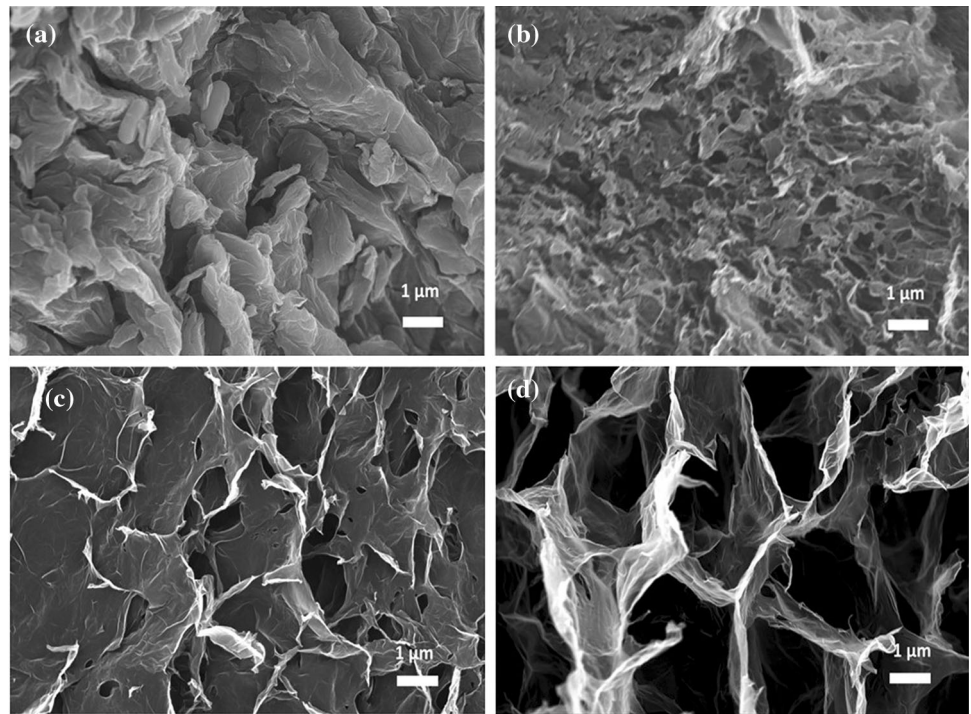


**Figure 7** Thermal gravimetric curves of aerogels.

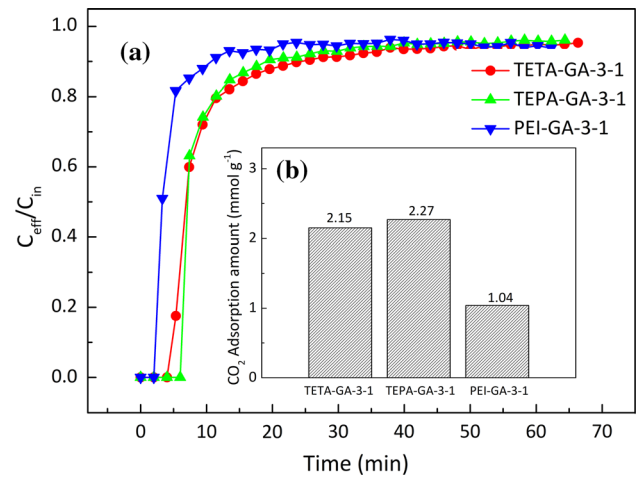


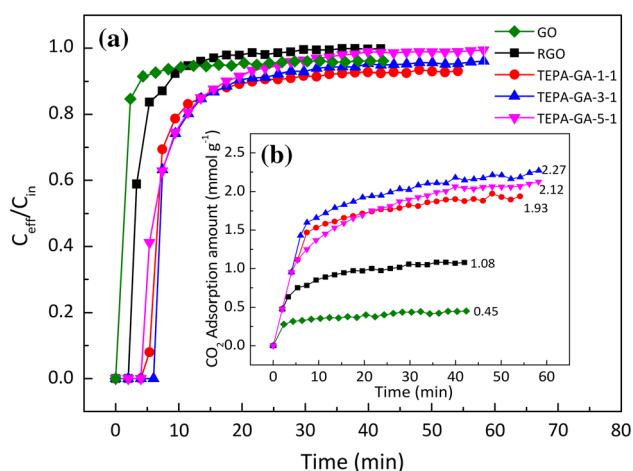
**Figure 8** The breakthrough curves (a) and adsorption capacities (b) of CO<sub>2</sub> adsorption on aerogels with different amines.

**Table 3** Elemental analysis results of aerogels with different amines

Samples	C (wt%)	H (wt%)	N (wt%)	N (mmol g <sup>-1</sup> )
TEPA-GA-3-1	71.83	4.04	11.15	7.96
TETA-GA-3-1	71.54	3.52	10.91	7.79
PEI-GA-3-1	70.54	3.62	10.09	7.21

GA-3-1 had higher N content than PEI-GA-3-1. What is more, the steric hindrance of high molecular weight PEI increased diffusion resistance of CO<sub>2</sub>, leading to poor CO<sub>2</sub> adsorption amount. Therefore, we chose TEPA as the optimal cross-linking agent for further research.

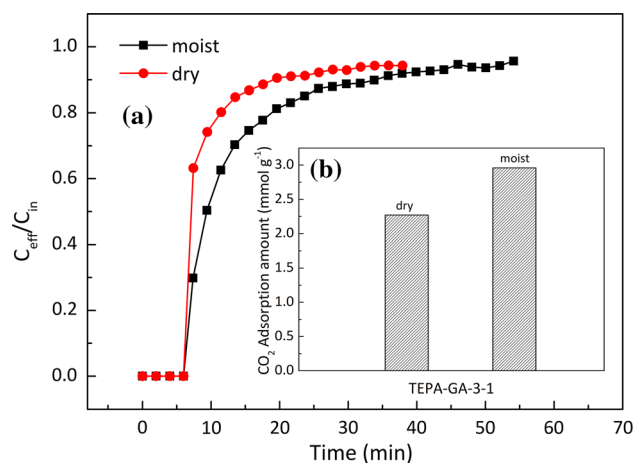
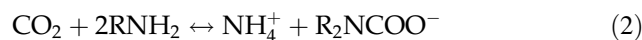
Considering the effect of organic amine type, we chose TEPA as cross-linker to investigate the influence of loading amount of TEPA on the adsorption capacity. The CO<sub>2</sub> adsorption amount was measured through analysis of breakthrough curves. As it is shown in Figure 9, compared with GO and RGO, TEPA-GA showed a higher CO<sub>2</sub> adsorption capacity. The CO<sub>2</sub> adsorption capacity increased at first and approached the maximum value when the mass ratio of TEPA to GO was equal to 3:1, and the equilibrium adsorption amount decreased when the mass ratio of TEPA to GO increased from 3:1 to 5:1. The CO<sub>2</sub> adsorption amount of TEPA-GA-3-1 could reach 2.27 mmol g<sup>-1</sup>, higher than other TEPA-GO aerogels. TEPA-GA-3-1 possessed relatively high N content (11.15 wt%) and large BET surface area (37 m<sup>2</sup> g<sup>-1</sup>), which could provide more active adsorption sites for

**Figure 9** The breakthrough curves (a) and adsorption capacities (b inset) of CO<sub>2</sub> adsorption on TEPA-GO aerogels.

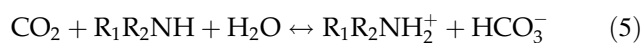
CO<sub>2</sub> capture when keeping a proper pore structure. Although TEPA-GA-5-1 had the highest N content among the adsorbents, its CO<sub>2</sub> adsorption amount was lower than that of TEPA-GA-3-1, which could account for pore blockage in TEPA-GA-5-1 (15 m<sup>2</sup> g<sup>-1</sup>). The excess TEPA would block the pores of the aerogel, negative to the further diffusion of CO<sub>2</sub> [31]. In addition, it can be found that the porous structure provided RGO better CO<sub>2</sub> adsorption property than GO. It is interesting that RGO had a higher BET surface area (168 m<sup>2</sup> g<sup>-1</sup>), but a lower CO<sub>2</sub> adsorption amount than TEPA-GA because of none amino groups. The introduction of TEPA provides more adsorption sites for chemical adsorption.

### Influence of water on the CO<sub>2</sub> adsorption

There is a certain amount of water vapor in the actual flue gas, so that it is important to study the effect of water vapor on CO<sub>2</sub> adsorption. As shown in Figure 10, TEPA-GA-3-1 displayed improved CO<sub>2</sub> adsorption capacity in the presence of water than that in the absence of water, indicating that the adsorbent was more favorable to adsorb CO<sub>2</sub> under wet condition. It has been reported that the solid amine adsorbents exhibit different adsorption mechanisms under wet and dry conditions, which can be described as follows [34]:

**Figure 10** The CO<sub>2</sub> adsorption breakthrough curves (a) and adsorption amounts (b) of TEPA-GA-3-1 under dry or wet condition.





According to the adsorption mechanisms above, adsorbing one mole  $\text{CO}_2$  requires two moles amino groups under dry condition, while only one mole amino group is needed under wet condition. As a result, TEPA-GA-3-1 achieved higher  $\text{CO}_2$  adsorption amount under wet condition.

### Regeneration performance of amine-modified graphene aerogels

From the perspective of economic benefits, the adsorbent with excellent recycling stability will be beneficial to practical industrial application. Based on the influence of organic amine type and the amount of TEPA, TEPA-GA-3-1 sample with the best adsorption capacity was selected for cyclic  $\text{CO}_2$  adsorption and desorption at adsorption temperature of 25 °C and desorption temperature of 90 °C. The adsorption breakthrough curves and adsorption capacities of the regenerated TEPA-GA-3-1 are shown in Figure 11. It can be found that the regenerated TEPA-GA-3-1 had a similar breakthrough curve with the fresh TEPA-GA-3-1, but showing a slight decrease of equilibrium  $\text{CO}_2$  adsorption capacity from 2.27  $\text{mmol g}^{-1}$  to 2.08  $\text{mmol g}^{-1}$ , which might be due to the leakage of amine compounds. The regeneration efficiency of TEPA-GA-3-1 remained nearly 91.6% of fresh sample after 6 cycles, implying that the adsorbent has a fair good

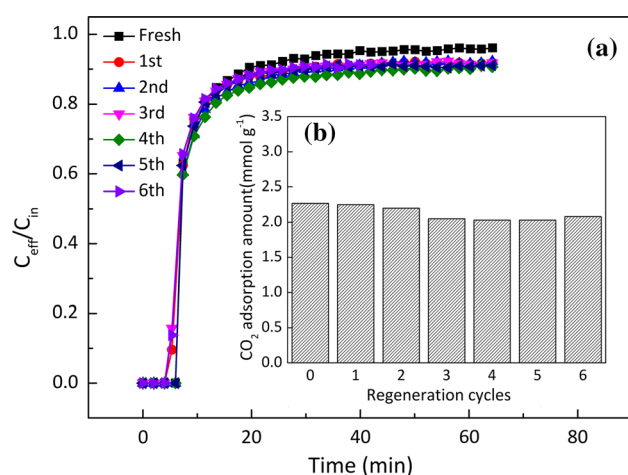


**Figure 11** The cyclic  $\text{CO}_2$  adsorption breakthrough curves (a) and adsorption amount (b) of TEPA-GA-3-1 aerogel.

**Table 4** Elemental analysis results of the fresh aerogel and regenerated aerogel

Adsorbent	Element content (wt%)		
	C	H	N
Fresh adsorbent	71.83	4.04	11.15
6th regeneration	70.91	4.44	10.90

regeneration performance. The excess TEPA physically attached on the surface of the aerogel partially lost during the cyclic desorption at high temperature (90 °C). The element analysis shown in Table 4 further verified the explanation, in which the N content decreased from 11.15 wt% (fresh) to 10.90 wt% (6th regeneration).

### Conclusion

In this study, three-dimensional porous graphene aerogels were successfully prepared via one-step hydrothermal method and freeze-drying, in which different organic amine reagents were used as cross-linker to combine graphene sheets. It is shown that organic amine type and the amount of the cross-linker had an effect on the structure of the aerogels and further affected the  $\text{CO}_2$  adsorption capacity. Among the amine-modified graphene aerogels, the prepared aerogel TEPA-GA-3-1 showed the highest  $\text{CO}_2$  adsorption capacity due to its large specific area, hierarchical porous structure as well as higher amino density. In addition, the existence of water improved its  $\text{CO}_2$  adsorption capacity (up to 2.96  $\text{mmol g}^{-1}$ ) because  $\text{H}_2\text{O}$  directly participates the reaction of  $\text{CO}_2$  with amine to form bicarbonates. After 6 times of adsorption–desorption cycles, the regeneration efficiency of the adsorbent could remain 91.6%, indicating that the graphene aerogels had fair good regeneration performance. Thus, the prepared graphene aerogels have a potential application for  $\text{CO}_2$  capture from flue gas.

### Acknowledgements

The authors gratefully acknowledge the financial support provided by the National Natural Science Foundation of China (Grant No. 51873238), Science

and Technology Project of Guangdong Province (sxm017, 2030218000189, 2019024).

## Declarations

**Conflict of interest** There are no conflicts to declare.

## References

- [1] Snoeckx R, Bogaerts A (2017) Plasma technology—a novel solution for CO<sub>2</sub> conversion? *Chem Soc Rev* 46:5805–5863. <https://doi.org/10.1039/c6cs00066e>
- [2] Singh G, Lee J, Karakoti A et al (2020) Emerging trends in porous materials for CO<sub>2</sub> capture and conversion. *Chem Soc Rev* 49:4360–4404. <https://doi.org/10.1039/d0cs00075b>
- [3] Tomé LC, Marrucho IM (2016) Ionic liquid-based materials: A platform to design engineered CO<sub>2</sub> separation membranes. *Chem Soc Rev* 45:2785–2824. <https://doi.org/10.1039/c5cs00510h>
- [4] Tan LS, Shariff AM, Lau KK, Bustam MA (2012) Factors affecting CO<sub>2</sub> absorption efficiency in packed column: A review. *J Ind Eng Chem* 18:1874–1883. <https://doi.org/10.1016/j.jiec.2012.05.013>
- [5] Singh G, Lakhi KS, Sil S et al (2019) Biomass derived porous carbon for CO<sub>2</sub> capture. *Carbon N Y* 148:164–186. <https://doi.org/10.1016/j.carbon.2019.03.050>
- [6] Brunetti A, Scura F, Barbieri G, Drioli E (2010) Membrane technologies for CO<sub>2</sub> separation. *J Memb Sci* 359:115–125. <https://doi.org/10.1016/j.memsci.2009.11.040>
- [7] Ma B, Lin R, He H et al (2020) Rapid synthesis of solid amine composites based on short mesochannel SBA-15 for CO<sub>2</sub> capture. *Compos Part B Eng* 185:107782. <https://doi.org/10.1016/j.compositesb.2020.107782>
- [8] Gong J, Lin H, Grygiel K, Yuan J (2017) Main-chain poly(ionic liquid)-derived nitrogen-doped micro/mesoporous carbons for CO<sub>2</sub> capture and selective aerobic oxidation of alcohols. *Appl Mater Today* 7:159–168. <https://doi.org/10.1016/j.apmt.2017.02.009>
- [9] Mendes PAP, Ribeiro AM, Gleichmann K et al. (2017) Separation of CO<sub>2</sub>/N<sub>2</sub> on binderless 5A zeolite. *J CO<sub>2</sub> Util* 20:224–233 <https://doi.org/10.1016/j.jcou.2017.05.003>
- [10] Yin F, Wu Z (2019) Synthesis of nitrogen-rich hollow microspheres for CO<sub>2</sub> adsorption. *J Mater Sci* 54:3805–3816. <https://doi.org/10.1007/s10853-018-3107-5>
- [11] Yuan D, Zhao D, Sun D, Zhou HC (2010) An isoreticular series of metal-organic frameworks with dendritic hexacarboxylate ligands and exceptionally high gas-uptake capacity. *Angew Chemie - Int Ed* 49:5357–5361. <https://doi.org/10.1002/anie.201001009>
- [12] Gadipelli S, Guo ZX (2015) Graphene-based materials: Synthesis and gas sorption, storage and separation. *Prog Mater Sci* 69:1–60. <https://doi.org/10.1016/j.pmatsci.2014.10.004>
- [13] Novoselov KS, Geim AK, Morozov SV et al (2004) Electric field effect in atomically thin carbon films. *Science* 306:666–669. <https://doi.org/10.1126/science.1102896>
- [14] Stankovich S, Dikin DA, Piner RD et al (2007) Synthesis of graphene-based nanosheets via chemical reduction of exfoliated graphite oxide. *Carbon N Y* 45:1558–1565. <https://doi.org/10.1016/j.carbon.2007.02.034>
- [15] Khodadadi Dizaji A, Mortaheb HR, Mokhtarani B (2016) Noncovalently functionalized graphene oxide/graphene with imidazolium-based ionic liquids for adsorptive removal of dibenzothiophene from model fuel. *J Mater Sci* 51:10092–10103. <https://doi.org/10.1007/s10853-016-0237-5>
- [16] Zhang Y, Huang LJ, Wang YX et al (2019) The preparation and study of ethylene glycol- modified graphene oxide membranes for water purification. *Polymers (Basel)* 11:1–12. <https://doi.org/10.3390/polym11020188>
- [17] Zhao Y, Ding H, Zhong Q (2012) Preparation and characterization of aminated graphite oxide for CO<sub>2</sub> capture. *Appl Surf Sci* 258:4301–4307. <https://doi.org/10.1016/j.apsusc.2011.12.085>
- [18] Pokhrel J, Bhorla N, Anastasiou S et al (2018) CO<sub>2</sub> adsorption behavior of amine-functionalized ZIF-8, graphene oxide, and ZIF-8/graphene oxide composites under dry and wet conditions. *Microporous Mesoporous Mater* 267:53–67. <https://doi.org/10.1016/j.micromeso.2018.03.012>
- [19] Balasubramanian R, Chowdhury S (2015) Recent advances and progress in the development of graphene-based adsorbents for CO<sub>2</sub> capture. *J Mater Chem A* 3:21968–21989. <https://doi.org/10.1039/c5ta04822b>
- [20] Yousefi N, Lu X, Elimelech M, Tufenkji N (2019) Environmental performance of graphene-based 3D macrostructures. *Nat Nanotechnol* 14:107–119. <https://doi.org/10.1038/s41565-018-0325-6>
- [21] Han Z, Tang Z, Sun Y et al (2015) Controllable synthesis of tetraethylenepentamine modified graphene foam (TEPA-GF) for the removal of lead ions. *Sci Rep* 5:1–8. <https://doi.org/10.1038/srep16730>
- [22] Liang J, Cai Z, Li L et al (2014) Scalable and facile preparation of graphene aerogel for air purification. *RSC Adv* 4:4843–4847. <https://doi.org/10.1039/c3ra45147j>
- [23] Chowdhury S, Balasubramanian R (2016) Three-Dimensional graphene-based porous adsorbents for postcombustion CO<sub>2</sub> Capture. *Ind Eng Chem Res* 55:7906–7916. <https://doi.org/10.1021/acs.iecr.5b04052>

- [24] Kuang Y, He H, Chen S et al (2019) Adsorption behavior of CO<sub>2</sub> on amine-functionalized polyacrylonitrile fiber. *Adsorption* 25:693–701. <https://doi.org/10.1007/s10450-019-00070-0>
- [25] Liu Z, Pudasainee D, Liu Q, Gupta R (2015) Post-combustion CO<sub>2</sub> capture using polyethyleneimine impregnated mesoporous cellular foams. *Sep Purif Technol* 156:259–268. <https://doi.org/10.1016/j.seppur.2015.10.009>
- [26] Meyer JC, Geim AK, Katsnelson MI et al (2007) The structure of suspended graphene sheets. *Nature* 446:60–63. <https://doi.org/10.1038/nature05545>
- [27] Sui ZY, Meng YN, Xiao PW et al (2015) Nitrogen-doped graphene aerogels as efficient supercapacitor electrodes and gas adsorbents. *ACS Appl Mater Interfaces* 7:1431–1438. <https://doi.org/10.1021/am5042065>
- [28] Zhang X, Sui Z, Xu B et al (2011) Mechanically strong and highly conductive graphene aerogel and its use as electrodes for electrochemical power sources. *J Mater Chem* 21:6494–6497. <https://doi.org/10.1039/c1jm10239g>
- [29] Hsiao MC, Liao SH, Yen MY et al (2010) Preparation of covalently functionalized graphene using residual oxygen-containing functional groups. *ACS Appl Mater Interfaces* 2:3092–3099. <https://doi.org/10.1021/am100597d>
- [30] Rasch F, Schütt F, Saure LM et al (2019) Wet-Chemical Assembly of 2D Nanomaterials into Lightweight, Microtube-Shaped, and Macroscopic 3D Networks. *ACS Appl Mater Interfaces* 11:44652–44663. <https://doi.org/10.1021/acsami.9b16565>
- [31] Liu F, Chen S, Gao Y, Xie Y (2017) CO<sub>2</sub> adsorption behavior and kinetics on polyethylenimine modified porous phenolic resin. *J Porous Mater*. <https://doi.org/10.1007/s10934-017-0375-4>
- [32] Sui ZY, Cui Y, Zhu JH, Han BH (2013) Preparation of Three-dimensional graphene oxide-polyethylenimine porous materials as dye and gas adsorbents. *ACS Appl Mater Interfaces* 5:9172–9179. <https://doi.org/10.1021/am402661t>
- [33] Liu Y, Sajjadi B, Chen WY, Chatterjee R (2019) Ultrasound-assisted amine functionalized graphene oxide for enhanced CO<sub>2</sub> adsorption. *Fuel* 247:10–18. <https://doi.org/10.1016/j.fuel.2019.03.011>
- [34] Yu J, Le Y, Cheng B (2012) Fabrication and CO<sub>2</sub> adsorption performance of bimodal porous silica hollow spheres with amine-modified surfaces. *RSC Adv* 2:6784–6791. <https://doi.org/10.1039/c2ra21017g>

**Publisher's Note** Springer Nature remains neutral with regard to jurisdictional claims in published maps and institutional affiliations.